

## Accepted Manuscript

### Feasibility Study of a Tungsten Wire Reinforced Tungsten Matrix Composite with $ZrO_x$ Interfacial Coatings

J. Du, T. Höschel, M. Rasinski, S. Wurster, W. Grosinger, J-H. You

PII: S0266-3538(10)00177-6  
DOI: [10.1016/j.compscitech.2010.04.028](https://doi.org/10.1016/j.compscitech.2010.04.028)  
Reference: CSTE 4708

To appear in: *Composites Science and Technology*

Received Date: 16 October 2009

Revised Date: 27 April 2010

Accepted Date: 30 April 2010

Please cite this article as: Du, J., Höschel, T., Rasinski, M., Wurster, S., Grosinger, W., You, J-H., Feasibility Study of a Tungsten Wire Reinforced Tungsten Matrix Composite with  $ZrO_x$  Interfacial Coatings, *Composites Science and Technology* (2010), doi: [10.1016/j.compscitech.2010.04.028](https://doi.org/10.1016/j.compscitech.2010.04.028)

This is a PDF file of an unedited manuscript that has been accepted for publication. As a service to our customers we are providing this early version of the manuscript. The manuscript will undergo copyediting, typesetting, and review of the resulting proof before it is published in its final form. Please note that during the production process errors may be discovered which could affect the content, and all legal disclaimers that apply to the journal pertain.



## Feasibility Study of a Tungsten Wire Reinforced Tungsten Matrix Composite with $ZrO_x$ Interfacial Coatings

J. Du<sup>1</sup>, T. Höschel<sup>1</sup>, M. Rasinski<sup>1,2</sup>, S. Wurster<sup>3</sup>, W. Grosinger<sup>3</sup>, J-H. You<sup>1\*</sup>

<sup>1</sup>Max-Planck-Institut für Plasmaphysik, EURATOM Association, Boltzmannstr. 2, 85748 Garching, Germany

<sup>2</sup>Warsaw University of Technology, Faculty of Materials Science and Engineering, ul. Woloska 141, 02-507 Warsaw, Poland

<sup>3</sup>Erich Schmid Institute of Materials Science of the Austrian Academy of Sciences, Jahnstrasse 12, A-8700 Leoben, Austria

### Abstract

Brittleness problem imposes a severe restriction on the potential application of tungsten as high-temperature structural material. In this paper, a novel toughening method for tungsten is proposed based on reinforcement by tungsten wires. The underlying toughening mechanism is analogous to that of fiber-reinforced ceramic matrix composites. Strain energy is dissipated by debonding and frictional sliding at engineered fiber/matrix interfaces. To achieve maximum composite toughness fracture mechanical properties have to be optimized by interface coating. In this work, we evaluated six kinds of  $ZrO_x$ -based interface coatings. Interfacial parameters such as shear strength and fracture energy were determined by means of fiber push-out tests. The parameter values of the six coatings were comparable to each other and satisfied the criterion for crack deflection. Microscopic analysis showed that debonding occurred mostly between the W filament and the  $ZrO_x$  coating. Feasibility of interfacial crack deflection was also demonstrated by a three-point bending test.

**Keywords:** A. Metal-matrix composites; B. Fracture toughness; B. Interfacial strength; B. Debonding; Fiber push-out test

\*Corresponding author:

e-mail) you@ipp.mpg.de, Phone) ++49 (0)89 3299 1373, Fax) ++49 (0)89 3299 1212

## 1. Introduction

Tungsten is currently the most favored candidate for the plasma-facing material of nuclear fusion reactors due to its refractory nature, excellent surface erosion resistance and good thermal conductivity. On the other hand, inherent brittleness and further embrittlement to be caused by neutron irradiation or recrystallization are the most critical drawbacks limiting its structural application. In this context, enhancement of the tungsten toughness has been one of the paramount R&D issues in the fusion reactor materials community. In general conventional metallurgical methods have been applied in order to improve the toughness including alloying with rhenium to increase ductility and severe plastic deformation or mechanical alloying followed by HIP to form a nanometer-sized microstructure [1-4]. Oxide particles dispersion could increase the creep strength but reduced the tensile elongation [2]. There is a strong restriction in the chemical composition of plasma-facing tungsten, because the requirements of plasma compatibility and reduced activation have to be fulfilled. This limitation impeded flexible application of various metallurgical options. In spite of intensive research efforts, the hitherto achieved progress is still distant from the design specifications. Microstructural instability at high temperatures and damage under intense neutron irradiation are the main challenges. Therefore, there is an urgent need to explore a novel toughening mechanism which is able to function under such fusion-relevant loading environment.

Since last two decades, active research efforts have been conducted to develop long fiber-reinforced ceramic matrix composites (FCMCs) for high-temperature structural applications. Toughness of FCMCs has been notably improved and overall mechanical performance was successfully approved in several industrial applications (e.g. brake disks of an aircraft or a racing car) [5-7]. The working principle of a high toughness FCMC is the non-plastic energy dissipation caused by controlled interfacial cracking and subsequent frictional sliding at the debonded fiber/matrix interface [5-8]. When a propagating primary matrix crack meets an array of fibers standing perpendicular to the crack faces, the primary crack can deflect along the vertical interfaces, provided a specific fracture mechanical condition is satisfied. Then the strong fibers collectively bridge the primary crack suppressing its dynamic extension. As the applied load is increased, the interfacial debonding may continue followed by fiber pull-out and the matrix crack opens further in a controlled manner. The total amount of the consumed energy is the measure of apparent toughness. The toughening mechanism of a FCMC is by now well understood in terms of fracture mechanics where fracture mechanical properties of interface are the determining parameters.

This toughening mechanism of FCMCs would also have validity for brittle tungsten provided that reinforcing fibers are strong enough and their interfaces are suitably engineered. Tungsten wire-reinforced tungsten matrix composite ( $W_f/W$ ) is a candidate. Commercially available tungsten wires are generally very strong (tensile strength:  $>2.7$  GPa) and quite ductile. This beneficial property is ascribable to extremely textured fine-grained structure. Hence the original toughness of tungsten wires can be utilized until the wires become fully embrittled during fusion operation. The amount of its contribution to the total toughness of a  $W_f/W$  composite will depend on the volume fraction of the wires. On the other hand, the overall chemical purity will be just slightly modified by interface coating because only thin ( $<1\mu\text{m}$ ) films are used. To author's knowledge there is no previous publication in literature dealing with this kind of tungsten composites prior to authors'. The idea of a novel  $W_f/W$  composite based on a fundamentally different toughening mechanism was the motivation of the present work [17, 18].

As in the FCMC technology, one of the major engineering challenges is how to optimize the interface coating. To this end, integrated evaluation of fracture mechanical and metallurgical behavior of the engineered interface is needed. A fiber push-out test can provide relevant material data and information on microscopic failure feature of an interface. In this paper we present the results of extensive fiber push-out experiments conducted on  $W_f/W$  composites either with  $ZrO_x$  single-layer or  $Zr/ZrO_x$  multi-layer interface coating. Single-filament mini-composite specimens were used. Interfacial parameters were determined by calibrating with theoretical equations. Microscopic analysis of the internal interface domains was carried out before and after a push-out test by means of scanning electron microscopy (SEM) and focused ion beam (FIB) preparation.

## 2. Experiment

### 2.1. Fabrication of composite specimens

A commercial tungsten (W) wire with diameter of  $150\mu\text{m}$  was used as fiber reinforcement. The W wire was wound on two square stainless steel frames (edges: 10 cm) with interval of a couple of millimeters and put into a magnetron sputtering device for coating the wire surface. Six different  $ZrO_x$  coatings were prepared as follows (see Figure 1):  $ZrO_x$  single-layer films with three different average thicknesses (150, 400, 900 nm, respectively), a  $ZrO_x$  single-layer film (140 nm) with a W protection film (140 nm), a  $Zr/ZrO_x$  multi-layer film (35 nm/55 nm each) and a  $W/ZrO_x$  multi-layer film (90 nm/90 nm each). Both multi-layer coatings consisted

of five  $ZrO_x$  films and five Zr or W films in an alternating way. Each of these coating layers shall form an engineered filament/matrix interface. The coated filaments were further coated with tungsten by CVD process using tungsten hexafluoride at  $550^\circ\text{C}$  to form a dense matrix mantle on the coated filaments. The fabricated single-filament  $W_f/W$  composite rods had a diameter of 2.5 mm and length of 35 mm. To produce push-out test specimens the cylindrical rods were carefully sliced into thin discs with four different thicknesses ranging from 50 to 300  $\mu\text{m}$  and finished by fine-polishing. It is generally expected that cutting of a composite rod into thin specimens would partially relax the residual stress. But this effect did not appear in our case since there was no residual thermal stress in the  $W_f/W$  composite. Figure 1 shows the longitudinal sections of the four different as-fabricated interface coatings. The micrographs exhibit intact adhesion between the individual layers. Porosity was found in the W protection film whereas the zirconium oxide layers were dense.

## 2.2. Push-out test

Fiber push-out test has been widely applied to probe the interface properties of various fiber-reinforced composites. At the same time theoretical models of push-out mechanics has been developed to interpret measured push-out responses and to calibrate interface parameters [9-16]. In this study we used an instrumented macro-indentation device ( $< 2\text{kN}$ ) for push-out test. Details of the device, specimen and test procedure are found elsewhere [17, 18].

In Figure 2 a typical push-out curve measured on a  $ZrO_x$  single-layer coating (140 nm) is plotted. The original load-displacement curve (no.1) is compared with the calibrated one (no.2) which was obtained by subtracting the machine compliance. The corresponding pushed-out filament is also shown in the box. The area below the curve indicates the total amount of work done by the applied load. The other coatings showed also similar characteristics in overall push-out responses.

In the initial loading phase the response was nearly linear elastic until it reached the maximum load  $P_d$  at the point B. Upon reaching  $P_d$ , interface cracking was initiated triggering rapid (40 ms) brittle shear rupture. At the same time, the stored elastic strain energy was released in sudden bursts causing a dynamic push-out movement from B to C until the filament was decelerated by frictional resistance. The displacement ( $d_o$ ) generated by this dynamic event was 32  $\mu\text{m}$ . A slight load jump was observed from C to D prior to the quasi-static progressive sliding stage which was caused by the delay of feedback signal to the load cell controller. Beyond the maximum friction load  $p_f$  at D frictional resistance decreased gradually as the

remaining contact area diminished. In this regime the applied work is mostly dissipated by cracking and frictional sliding at the interfaces. Push-out test was repeated five times for each specimen thickness.

### 2.3. Calibration of material parameters

The estimated material parameters of the interfaces are shear strength  $\tau_d$ , radial roughness stress  $\sigma_r$ , friction coefficient  $\mu$ , (roughness-induced) frictional shear stress  $\tau_r$  and fracture energy (toughness)  $\Gamma_i$ . These parameters were calibrated by means of numerical regression using the theoretical equations of selected shear-lag models (cf. Appendix) [17, 18].

$\tau_d$  is defined as the maximum value average shear stress attains at push-out load  $P_d$  before an interface begins to fail.  $\tau_d$  was calibrated by fitting the measured  $P_d$  vs.  $H$  data with eq.(A1), where  $H$  denotes the specimen thickness.

During the shearing motion of a debonded filament the asperity mismatch between two contacting faces generates strain oriented normal to the interface. We call the corresponding stress radial roughness stress  $\sigma_r$ .  $\sigma_r$  and friction coefficient  $\mu$  were calibrated by fitting the measured  $P_{fr}$  vs.  $l$  data with eq.(A2), where  $l$  denotes the embedded filament length at  $P_{fr}$  ( $l = H - d_o$ ). The frictional shear stress  $\tau_r$  was calculated using the relation  $\tau_r = \mu \cdot \sigma_r$ .

Fracture energy  $\Gamma_i$  (mode II) was calibrated by fitting the measured  $p$  vs.  $H$  data with eq.(A4) where  $p = P_d / (\pi r_f^2)$ .

## 3. Results and discussion

### 3.1. Interfacial parameters

In Figures 3, 4 and 5 the experimental data of the W/ZrO<sub>x</sub> single-layer coating are plotted as an example to illustrate a generic feature of the parameter calibration procedure. All other coatings also exhibited a similar feature, thus are not presented separately. Each graph shows the  $P_d$  vs.  $H$ ,  $P_{fr}$  vs.  $l$  and  $p$  vs.  $H$  data, respectively, together with the corresponding regression curves produced using eqs.(A1), (A2) and (A4). The final result of calibration is summarized in Table 1. In addition, recently published literature data of other coating systems for W<sub>f</sub>/W composite are also listed. The literature data include carbon single-layer film, copper/tungsten single-layer film and copper/tungsten multi-layer film. It is noted that the scattering errors were relatively small for all data.

In terms of magnitude of the parameters, a systematic trend is not clearly appreciable in Table 1. As a whole the calibrated parameter values of the ZrO<sub>x</sub>-based coatings were comparable with each other except for the Zr/ZrO<sub>x</sub> multi-layers. The latter produced essentially smaller  $\tau_d$  and  $\Gamma_i$  values ( $\tau_d$ : 330 MPa,  $\Gamma_i$ : 1.2 J/m<sup>2</sup>) than the other coatings.  $\tau_d$  of the ZrO<sub>x</sub> single layer and the W/ZrO<sub>x</sub> single-/multi-layer coatings ranged from 360 to 440 MPa whereas  $\Gamma_i$  ranged between 3 and 6 J/m<sup>2</sup>. Apart from the Zr/ZrO<sub>x</sub> multi-layers, there seems to be no definite evidence of any multi-layer effect or thickness dependence.  $\Gamma_i$  of the ZrO<sub>x</sub> single-layer was also calibrated using eq.(A5). The two values agreed well with each other within 2.4 % error. All ZrO<sub>x</sub>-based coatings exhibited rather uniform and large values of  $\mu$  (>1) indicating a significant contribution of roughness. One of its physical origins is the small debris of the coating film attached on the broken interfaces as shown in Figure 6. In addition, the tungsten filaments have inherent surface asperity produced by the wire drawing process. Normally the interface of a FCMC has smaller  $\mu$  values ranging between 0.1~0.6 because ceramic fibers have a smooth surface.

In the case of the carbon coating, its  $\tau_d$ ,  $\tau_r$  and  $\mu$  were significantly smaller compared to the ZrO<sub>x</sub>-based coatings but its  $\Gamma_i$  was larger. This feature indicates a lubricating property of the carbon film.

As to the copper-based coatings, the W/Cu multi-layers showed a similar range of parameter values as the ZrO<sub>x</sub> single layer coatings. The Cu single layer (170 nm) with two W protection films on both sides (50 nm) had particularly large values of  $\Gamma_i$  and  $\sigma_r$  whereas its  $\tau_d$  and  $\mu$  were comparable to those of the ZrO<sub>x</sub>-based coatings. Electron micrograph revealed that the thin Cu films ruptured without any notable plastic flow in contrast to the thicker counterpart (420 nm) which underwent extensive plastic deformation [17]. The brittle rupture behavior of the thin copper film is due to the limitation of dislocation glide path. The parameters of the thicker Cu film could not be evaluated within the linear elastic shear-lag models.

One important implication of the estimated  $\Gamma_i$  data is that they satisfy the fracture-mechanical criterion for crack deflection at the interface. According to the pioneering work of He and Hutchinson [19], interfacial cracking in a bi-material bond joint under tension requires that the ratio  $\Gamma_i/\Gamma_f$  be smaller than a specific value depending on elastic mismatch between the two bonding partners. Here,  $\Gamma_f$  denotes the fracture toughness of the material in front of an approaching crack. If the elastic mismatch is negligible as in the present case where both fiber

and matrix are tungsten, then the critical value is reduced to 0.25. But it is noted that this value was originally derived for a flat interface. The  $\Gamma_f$  value of a commercially available tungsten wire is typically about 300 J/m<sup>2</sup> [20]. Substituting this value and the  $\Gamma_i$  data into the criterion above, one finds that the requirement of crack deflection along interface is obviously satisfied ( $\Gamma_i/\Gamma_f$  : 0.01~0.02). It is well known that the capability of energy absorption (a measure of toughness) of a FCMC is actually determined by this ratio.

### 3.2. Microscopic investigation

Figure 7 (a) shows a part of the pushed-out filament which was originally coated with the W/ZrO<sub>x</sub> single-layer coating. In the box (b) the coating film detached from the filament is shown in higher magnification. (c) shows the longitudinal section of the debonded interface domain after test. The base part of the exposed filament was locally excavated by FIB as shown in the box (d) to observe the interior domain of the interface. In both micrographs it is seen that the separation occurred articulately at the W filament/ZrO<sub>x</sub> interface. Both the ZrO<sub>x</sub> coating and the W film remained attached to the W matrix side. The exposed surface of the pushed-out filament looked completely uncovered. Such a clear debonding feature suggests absence of chemical bonding between the ZrO<sub>x</sub> film and the filament. The load carrying capability of the interface under shearing was controlled by interlocking of roughness as well as adhesion. The calibrated  $\tau_d$  value of the ZrO<sub>x</sub>/filament interface has to be interpreted as effective shear strength averaged over the length. The bonding at the W film/ZrO<sub>x</sub> interface and the W film/W matrix interface was fully intact.

Figure 8 shows the pushed-out filaments of the ZrO<sub>x</sub> single-layer coatings with three different thicknesses (a: 150 nm, b: 400 nm, c: 900 nm) together with the longitudinal sections of the corresponding interface domains. It is seen that the filament surface with the 150 nm ZrO<sub>x</sub> coating was only partly covered indicating that the bond strength at both sides of the ZrO<sub>x</sub> film were comparable. On the contrary, the thicker ZrO<sub>x</sub> coatings (b, c) showed a debonding feature identical to the aforementioned W/ZrO<sub>x</sub> single-layer coating case. However, the measured parameters of the 900 nm coating did not coincide well with those of the W/ZrO<sub>x</sub> single-layer coating in spite of the similarity in their microstructural fracture feature. On the other hand, the analogy of the parameters between the 150 nm coating and the W/ZrO<sub>x</sub> single-layer coating was a rather unexpected outcome since the failure features of the two coatings were quite different. A columnar grain structure is visible at the matrix side of the 900 nm coating.



Figure 9 (a) shows the exposed surface of the pushed-out filament with the ZrO<sub>x</sub>/Zr multi-layer coating. Also shown are the longitudinal interface sections at two different locations (b, c). The micrographs reveal that debonding occurred either at the filament/multilayer interface or at the multilayer/W matrix interface with similar failure probability. Hence the calibrated parameters are actually averaged properties of the two adhesion interfaces. The dual cracking behavior may explain the particularly smaller magnitude of  $\tau_d$  and  $\Gamma_i$ . The number of favored failure sites was approximately doubled increasing the failure probability and thus decreasing the strength. The multi-layer coating itself and the multi-layer/W film bonding remained intact.

Figure 10 shows the pushed-out filament of the W/ZrO<sub>x</sub> multi-layer coating (a) and magnified views of the multi-layer at the ruptured interface (b: cross section, c: longitudinal section). A part of the coating remained attached to the filament near the edge, but the filament surface was mostly uncovered. The multi-layer coating was still bonded to the W matrix side even after the filament/coating(ZrO<sub>x</sub>) interface was separated. It is also found that the multi-layer itself and the coating(ZrO<sub>x</sub>)/matrix interface were partly fractured. But the bond interfaces within the W/ZrO<sub>x</sub> multi-layer coating seem to be intact.

Incidentally, stability of the microstructure at high temperatures or under neutron irradiation is an open issue needing further clarification. Recently authors' group is performing extensive push-out tests on selected oxide coating interfaces after annealing at 800 °C for 10 hours to investigate thermal impact. Yet, the result of this ongoing work is not included in the present article.

### 3.3. Direct validation of interfacial crack deflection

In previous section it was demonstrated that the calibrated  $\Gamma_i$  values of the tested coatings satisfied the fracture-mechanical criterion of interfacial crack deflection. For direct visual validation of this prediction a 3-point mini bending test was conducted under in-situ SEM observation using a miniaturized single-filament specimen. To trace the crack propagation, the originally rod-shaped model composite (with Zr/ZrO<sub>x</sub> multi-layer coating) was cut along the longitudinal axis. For stable supporting of the half cylinder specimen during bending test, the two lateral edges were cut out to produce parallel side faces. The surface of the cut

sections was fine polished. A sharp notch was introduced on one lateral face to define the crack initiation site.

Figure 11 shows the cut section of a half-cylindrical mini specimen set up in a testing device after bending test. A schematic illustration is also attached. Until the applied load reached 110 N there was no sign of any failure. At 110 N a transverse crack was abruptly produced from the notch root and propagated rapidly in opening mode perpendicular to the specimen axis but without cutting the filament. The sharp crack plane extended through the matrix surrounding the wire. Figure 12 shows the cracked interface domain with higher magnification. The two micrographs clearly reveal that the primary matrix crack was deflected along the interface leading to controlled debonding at the interface while the filament bridged the opening crack. This cracking feature coincides exactly with the typical toughening mechanism of a CMC. This result may be a direct evidence to support our approach to realize a high-toughness tungsten composite material.

#### 4. Conclusions

1. The fracture energy and shear strength of the filament/matrix interface in  $W_f/W$  composites could be determined using the measured push-out test data and numerical fitting to theoretical equations.
2. The values of the interfacial parameters obtained for six different  $ZrO_x$ -based coatings were comparable with each other. In the cases of the  $ZrO_x$  single layer and the  $W/ZrO_x$  single- and multi-layer coatings, the calibrated shear strength  $\tau_d$  ranged from 360 to 440 MPa whereas the fracture energy  $\Gamma_i$  ranged between 3 and 6 J/m<sup>2</sup>. On the other hand, the  $Zr/ZrO_x$  multi-layer coating showed notably smaller magnitude for both parameters. ( $\tau_d$ : 330 MPa,  $\Gamma_i$ : 1.2 J/m<sup>2</sup>) The estimated  $\Gamma_i$  values satisfied the fracture mechanical criterion for interfacial crack deflection.
3. The cracking and separation occurred mostly at the filament/ $ZrO_x$  coating interface while both the  $ZrO_x$  coating and the W film remained attached to the W matrix side. On the contrary, in the  $Zr/ZrO_x$  multi-layer case, debonding occurred equally either at the filament/coating or the coating/matrix interface.
4. The exposed surface of the pushed-out filament was fully uncovered suggesting absence of any strong chemical bonding between the  $ZrO_x$  film and the W filament.

5. The capability of the interfacial  $ZrO_x$  coating to allow controlled crack deflection along the interface under tensile load could be demonstrated in a 3-point bending test on a miniaturized single-filament specimen. This crack bridging behavior of the coated filament can be regarded as more direct evidence supporting the  $W_f/W$  toughening concept.

### Acknowledgement

The author J. Du is grateful to Chinese Scholarship Council (CSC) for the financial support.

### References

- [1] Lässer R, Baluc N, Boutard J.-L, Diegele E, Dudarev S, Gasparotto M, Möslang A, Pippan R, Riccardi B, van der Schaaf B. Structural materials for DEMO: The EU development, strategy, testing and modeling. *Fus Engng Des* 2007; 82: 511-520.
- [2] Rieth M, Dafferner B. Limitations of W and W-1%La<sub>2</sub>O<sub>3</sub> for use as structural materials. *J Nucl Mater* 2005; 342: 20-25.
- [3] Faleschini M, Kreuzer H, Kiener D, Pippan R. Fracture toughness investigations of tungsten alloys and SPD tungsten alloys. *J Nucl Mater* 2007; 367-370: 800-805.
- [4] Kurishita H, Amano Y, Kobayashi S, Nakai K, Arakawa H, Hiraoka Y, Takida T, Takebe K, Matsui H. Development of ultra-fine grained W-TiC and their mechanical properties for fusion applications. *J Nucl Mater* 2007; 367-370: 1453-1457.
- [5] Chawla KK. *Ceramic Matrix Composites*, London, UK: Chapman & Hall, 1993. p. 181-190, p. 296-336.
- [6] Evans A G. Design and life prediction issues for high-temperature engineering ceramics and their composites. *Acta Mater* 1997; 45: 23-40.
- [7] Evans A G. Perspective on the development of high-toughness ceramics. *J Am Ceram Soc* 1990; 73(2): 187-206.
- [8] Budiansky B, Evans A G, Hutchinson J W. Fiber-matrix debonding effects on cracking in aligned fiber ceramic composites, *Int J Solids Structures* 1995; 32: 315-328.
- [9] Greszczuk L B. Theoretical studies of the mechanics of fiber-matrix interface in composites. *Interface in composite*, ASTM special technical publication 1969; 452: 42-58.
- [10] Shetty D K. Shear-lag analysis of fiber push-out (indentation) tests for estimating interfacial friction stress in ceramic-matrix composites. *J Am Ceram Soc* 1988; 71(2): C-107-C-109.

- [11] Parthasarathy T A, Jero P D, Kerans R J. Extraction of interface properties from a fiber push-out test. *Scripta Metall Mater* 1991; 25: 2457-2462.
- [12] Liang C, Hutchinson J W. Mechanics of the fiber pushout test. *Mech Mater* 1993; 14: 207-221.
- [13] Kalton A F, Howard S J, Janczak-Rusch J, Clyne T W. Measurement of interfacial fracture energy by single fiber push-out testing and its application to the titanium-silicon carbide system. *Acta Mater* 1998; 46: 3175-3189.
- [14] Kerans R J, Hay R S, Pagano N J, Parthasarathy T A. The role of the fiber-matrix interface in ceramic composites. *Ceram Bull* 1989; 68(2): 429-442.
- [15] Jero P D, Kerans R J. The contribution of interfacial roughness to sliding friction of ceramic fiber in a glass matrix. *Scripta Metall Mater* 1990; 24: 2315-2318.
- [16] Kerans R J, Parthasarathy T A. Theoretical analysis of the fiber pull-out and push-out tests. *J Am Ceram Soc* 1991; 74(7): 1585-1596.
- [17] Du J, Höschel T, Rasinski M, You J H. Interfacial fracture behavior of tungsten wire/tungsten matrix composites with copper-coated interfaces. *Mater Sci Eng A* 2009; 527: 1623-1629.
- [18] Du J, Höschel T, Rasinski M, You J.H. Shear debonding behavior of a carbon-coated interface in a tungsten fiber-reinforced tungsten matrix composite. *J Nucl Mater* 2010; in press.
- [19] He M Y, Hutchinson J W, Crack deflection at an interface between dissimilar elastic materials. *Int J Solids Struct* 1989; 25(9): 1053-1067.
- [20] Conner R D, Dandliker R B, Johnson W L, Mechanical properties of tungsten and steel fiber reinforced  $Zr_{41.25}Ti_{13.75}Cu_{12.5}Ni_{10}Be_{22.5}$  metallic glass matrix composites. *Acta mater* 1998; 46(17): 6089-6102.

## Appendix

### A.1. Interfacial shear strength $\tau_d$

Greszczuk [9] suggested a relationship between the debonding load  $P_d$  and the shear strength  $\tau_d$  based on the shear-lag theory of pull-out test.

$$P_d = \frac{2\pi r_f \tau_d}{\alpha} \tanh(\alpha L) \quad (A1)$$

where,  $P_d$ : the applied load at the onset moment of interface debonding,  $r_f$ : the filament radius,  $\alpha$ : the shear-lag parameter depending on the elastic properties of the fiber and the matrix and  $L$ : the initially embedded filament length. This equation can also be used for a push-out test case by replacing  $L$  with the specimen thickness  $H$  because eq.(A1) assumes rapid crack extension at  $\tau_d$  in a thin specimen.

#### A.2. Roughness stress $\sigma_r$ and friction coefficient $\mu$

According to the shear-lag model of Shetty [10],  $P_{fr}$  can be correlated with  $L$  as follows:

$$P_{fr} = \frac{\pi r_f^2 \sigma_r}{k} (e^\zeta - 1) \quad (A2)$$

where  $\zeta = 2\mu k l / r_f$  and  $k = E_m \nu_f / E_f (1 + \nu_m)$ , where  $\nu$  and  $E$  are the Poisson ratio and the Young's modulus, respectively. The subscripts f and m stand for filament and matrix.  $\sigma_r$  is thermal expansion mismatch which is negligible in the present case.

On the other hand, Liang and Hutchinson [12] argued that  $\tau_r$  was a constant friction term arising from an asperity mismatch at a broken interface. They suggested

$$P_{fr} = \frac{\pi r_f^2 \tau_r}{\mu B_1} (e^\xi - 1) \quad (A3)$$

where  $\xi = 2\mu B_1 L / r_f$ ,  $B_1 = \nu_f E_m / [(1 - \nu_f) E_m + (1 + \nu_m) E_f]$ .

#### 3.4. Interfacial fracture toughness $\Gamma_i$

Liang and Hutchinson [12] developed a model to calibrate the interfacial fracture toughness  $\Gamma_i$  (mode II) from a push-out test data which is expressed as

$$p = p_R + 2 \left( \frac{\Gamma_i E_f}{B_2 r_f} \right)^{0.5} e^\xi + \frac{\tau_r}{\mu B_1} (e^\xi - 1) \quad (A4)$$

where  $p = P_d / (\pi r_f^2)$  and  $B_2 = 1 - 2\nu_f B_1$ .  $p_R$  denotes the axial thermal residual stress and thus becomes null for the present case. It is noted that the third term of the right hand side is identical to eq. (A3). The second term stands for the contribution of the interfacial fracture energy to the debonding resistance.

Alternatively, Clyne suggested a model for the interface fracture toughness [13] based on an energy balance approach. This model yielded a relationship between  $\Gamma_i$  and  $p$  as

$$\Gamma_i = \frac{r_f}{4E_f} [(p - \sigma_z^{th}) e^{-\xi} + \frac{\tau_r^0}{\mu B_1} (e^{-\xi} - 1)]^2 \quad (A5)$$

where  $\sigma_z^{\text{th}}$  represents the axial thermal residual stress and  $\tau_r^o$  the total shear stress consisting of the contributions from roughness and thermal strain. Again, the contribution of thermal stress vanishes. Eq. (A5) has exactly the same form as eq. (A4) except for the factor  $B_2$ .

ACCEPTED MANUSCRIPT

**Figure captions**

Figure 1. Longitudinal sections of the as-fabricated interfaces with four different coatings. (a)  $ZrO_x$  single-layer film, (b)  $ZrO_x$  single-layer film with a W protection film, (c) Zr/ $ZrO_x$  multi-layer film and (d) W/ $ZrO_x$  multi-layer film.

Figure 2. A typical push-out curve measured on a  $ZrO_x$  single-layer coating (140 nm) together with a SEM image of the pushed out filament. Curve 1: original load-displacement curve, Curve 2: after correction of machine compliance.

Figure 3. Collected  $P_d$  vs.  $H$  data obtained from the push-out curves of  $ZrO_x$  single-layer coating together with the corresponding regression curve based on eq.(A1).

Figure 4. Collected  $P_{fr}$  vs.  $l$  data obtained from the push-out curves of  $ZrO_x$  single-layer coating together with the corresponding regression curve based on eq.(A2).

Figure 5. Collected  $p$  vs.  $H$  data obtained from the push-out curves of  $ZrO_x$  single-layer coating together with the corresponding regression curve based on eq.(A4).

Figure 6. Small debris of the coating film attached on a broken interface.

Figure 7. (a) A part of the pushed-out filament which was originally coated with W/ $ZrO_x$  single-layer coating, (b) coating film detached from the filament in higher magnification, (c) longitudinal section of the debonded interface layer, (d) locally excavated filament base and exposed interior interface domain (FIB preparation)

Figure 8. Pushed-out filaments of  $ZrO_x$  single-layer coatings with three different thicknesses (a: 150 nm, b: 400 nm, c: 900 nm) together with the longitudinal sections of their corresponding interface domains.

Figure 9. (a) Exposed surface of the pushed-out filament with  $ZrO_x/Zr$  multi-layer coating, (b, c) longitudinal interface sections at two different locations.

Figure 10. (a) Pushed-out filament of W/ZrO<sub>x</sub> multi-layer coating, magnified views of the multi-layers at the ruptured interface (b: cross section, c: longitudinal section).

Figure 11. Cut section of a half-cylindrical mini specimen with Zr/ZrO<sub>x</sub> multi-layer interface coating set up in a testing device after bending test. The vertical crack was initiated at the applied load of 110 N.

Figure 12. Interface domain of the half-cylindrical bending specimen with higher magnification. Interface debonding crack is clearly seen.

ACCEPTED MANUSCRIPT



Table 1. Estimated interfacial parameters

coatings (present study)		$\tau_d$ (MPa)	$\tau_r$ (MPa)	$\sigma_r$ (MPa)	$\mu$	$\Gamma_i$ (J/m <sup>2</sup> )
single layer	W/ZrO <sub>x</sub> (140nm/140nm)	359±10	136	106±11	1.3±0.1	3.0±0.4
	ZrO <sub>x</sub> (150nm)	394±12	110	57±8	1.9±0.1	2.9±0.5
	ZrO <sub>x</sub> (400nm)	441±8	127	85±5	1.5±0.0	3.0±0.3
	ZrO <sub>x</sub> (900nm)	433±9	111	73±7	1.5±0.1	5.9±0.9
multi layer	W/ZrO <sub>x</sub> (90nm/90 nm)	413±13	175	146±7	1.2±0.0	3.5±0.6
	Zr/ZrO <sub>x</sub> (35nm/50nm)	328±9	104	60±4	1.7±0.1	1.2±0.2
coatings (previous study)						
single layer	C (600nm) <sup>a</sup>	285±5	74	71±8	1.0±0.1	7.4±0.7
	W/Cu/W (420nm) <sup>b</sup>	384±5				
	W/Cu/W (170nm)	412±5	176	225±46	0.8±0.1	12.3±1.4
multi layer	W/Cu (110nm/55nm) <sup>b</sup>	429±6	86	58±4	1.5±0.1	7.7±0.7

<sup>a</sup>: [18], <sup>b</sup>: [17], the presented data are modified one using an improved fitting algorithm.

Figure1

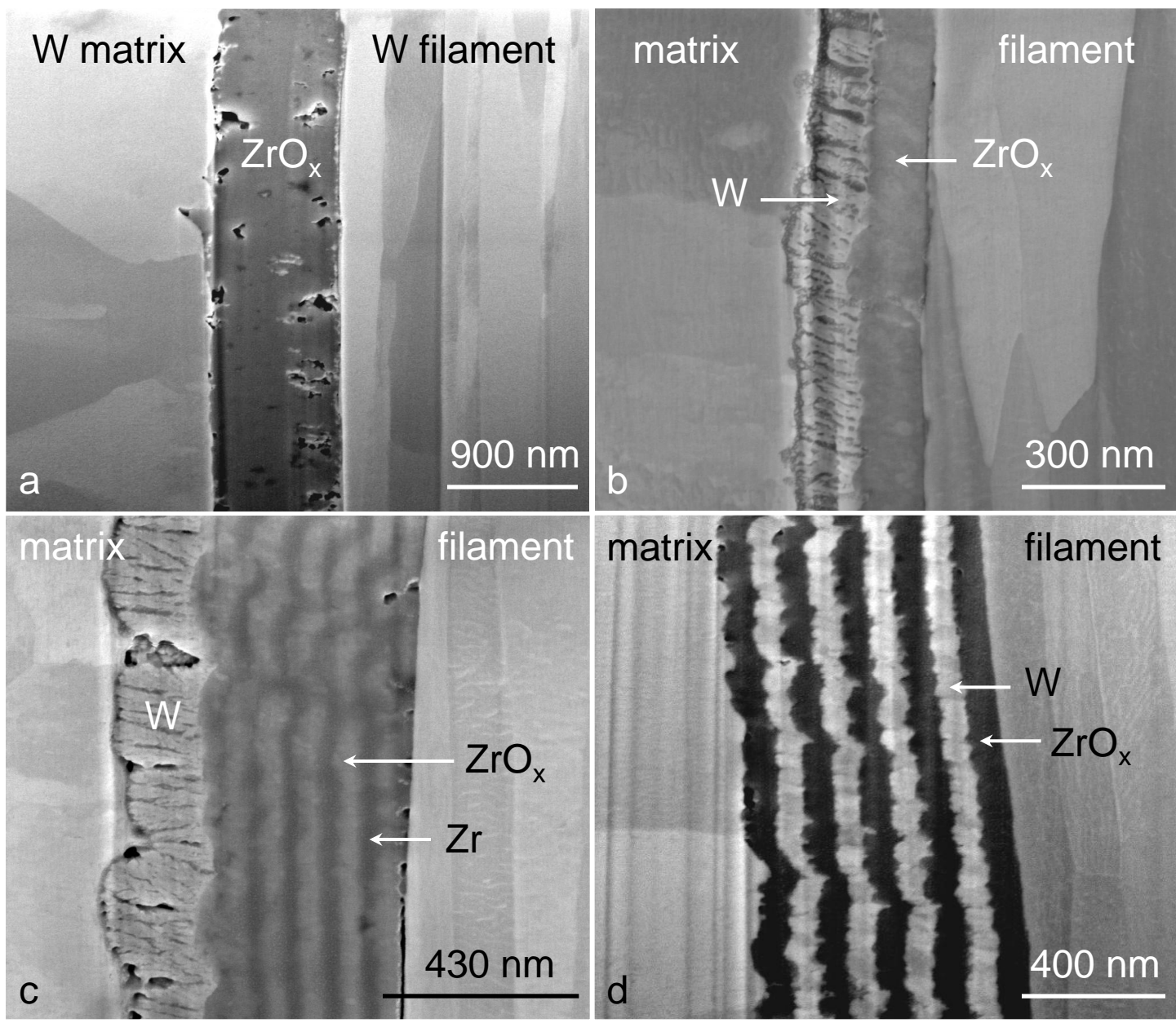


Figure2

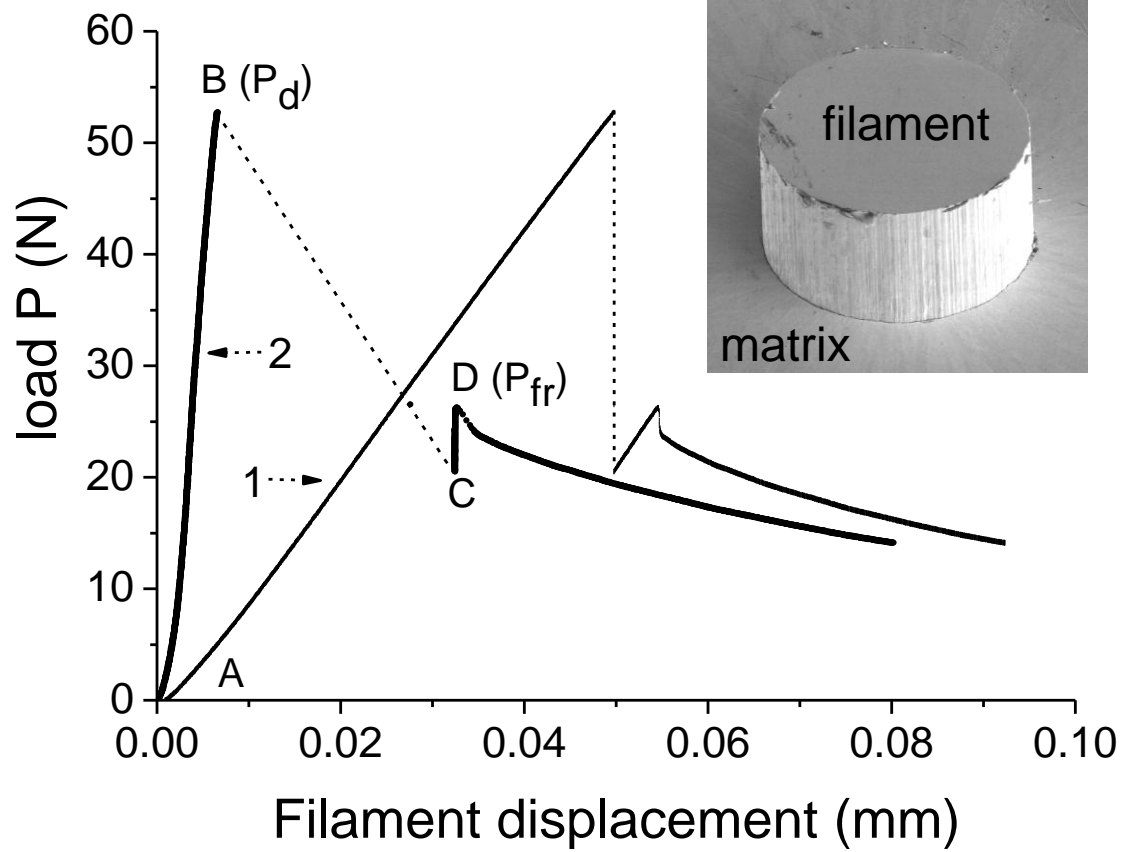


Figure3

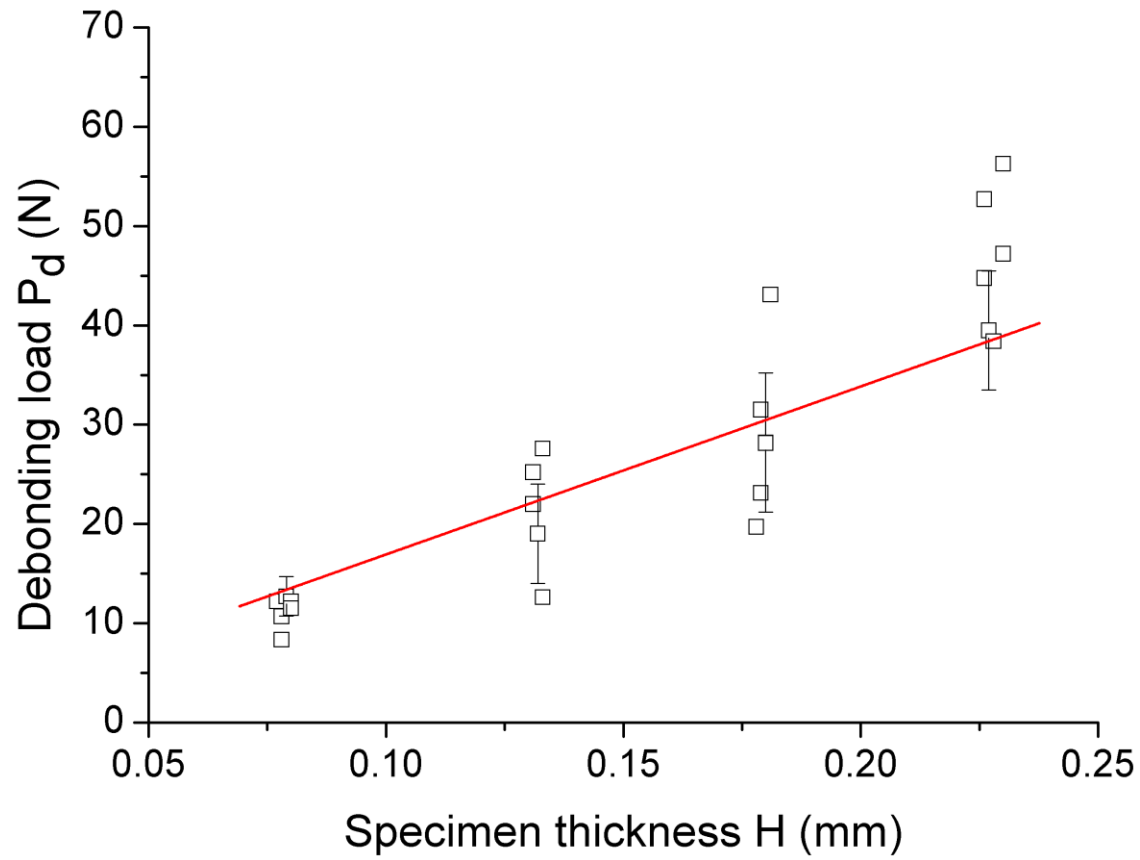


Figure4

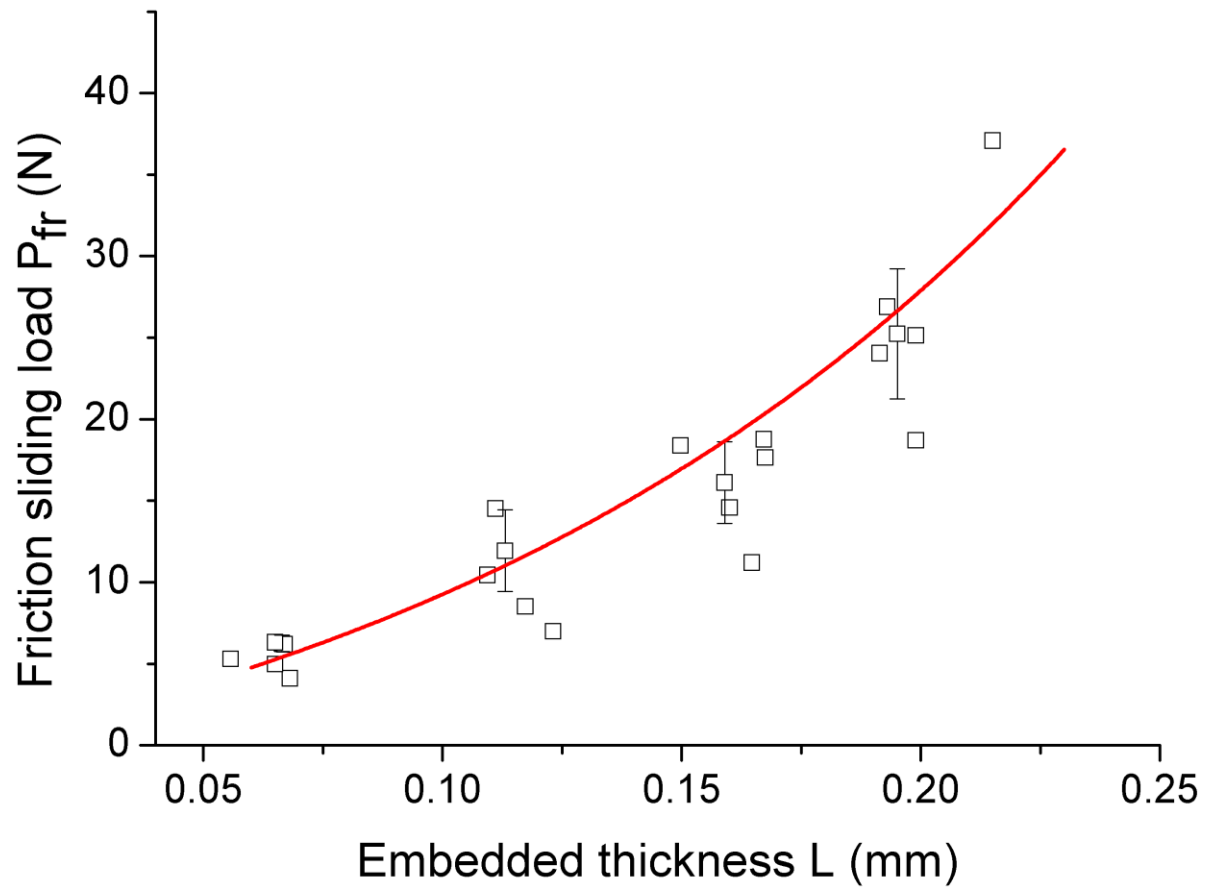


Figure5

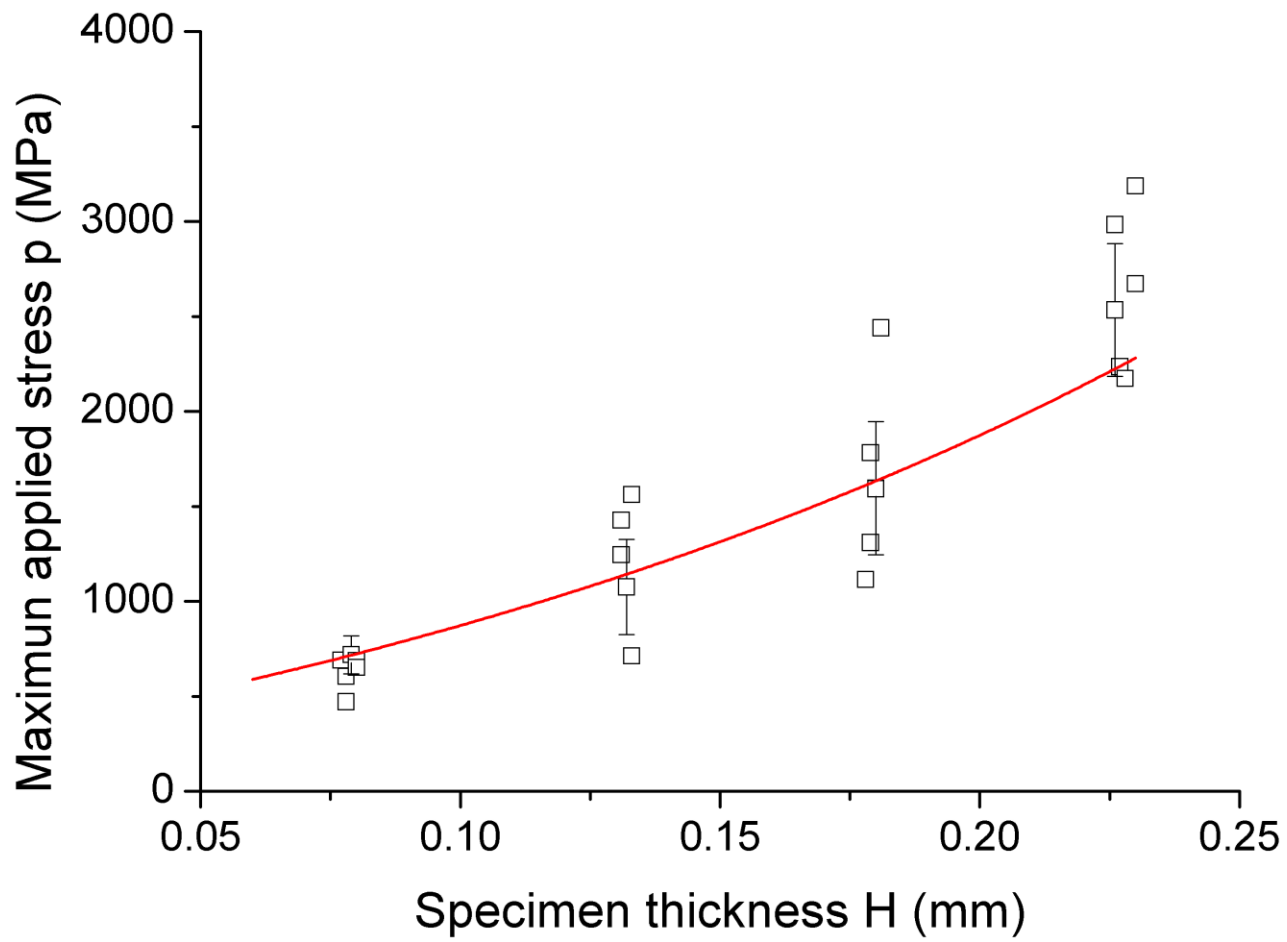


Figure6

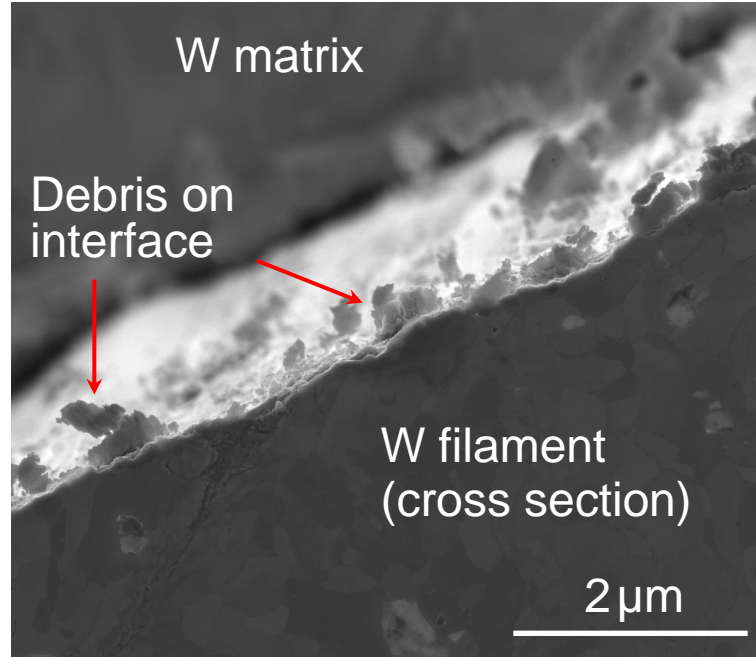


Figure 7

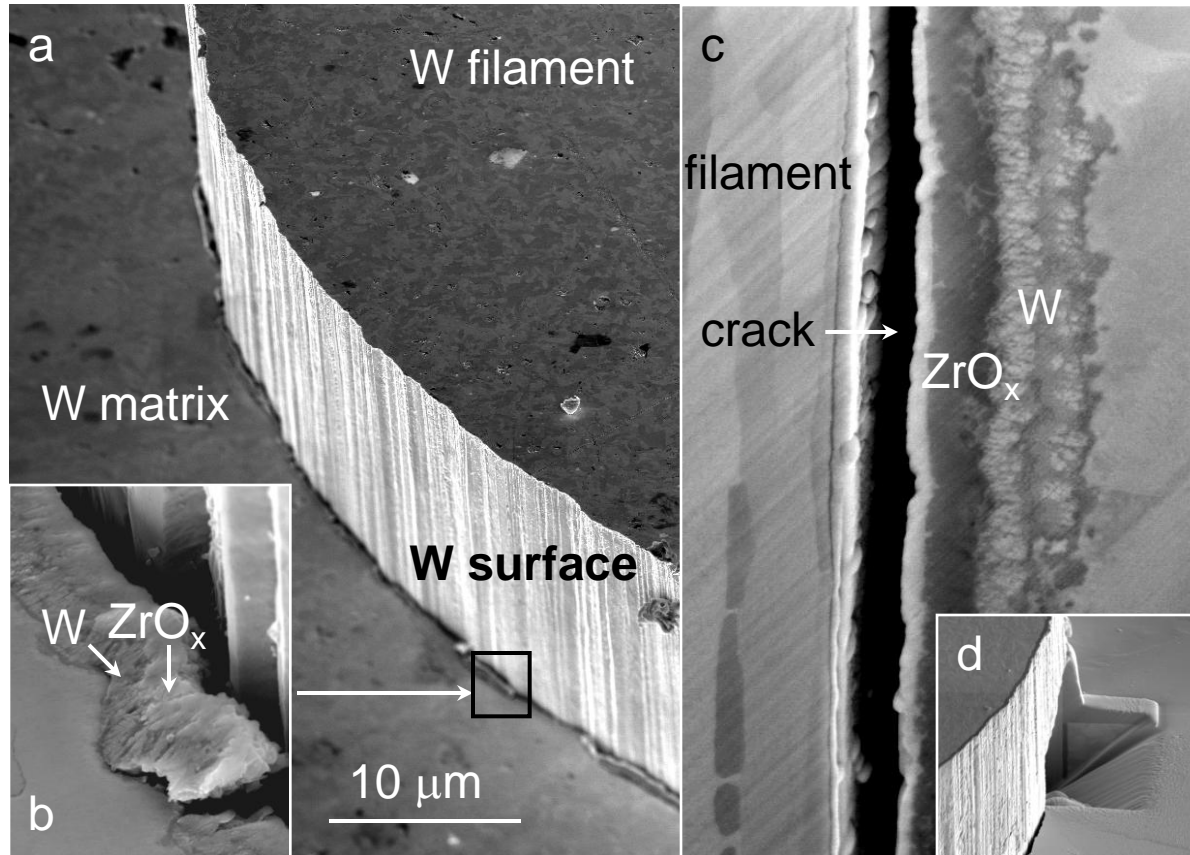




Figure8

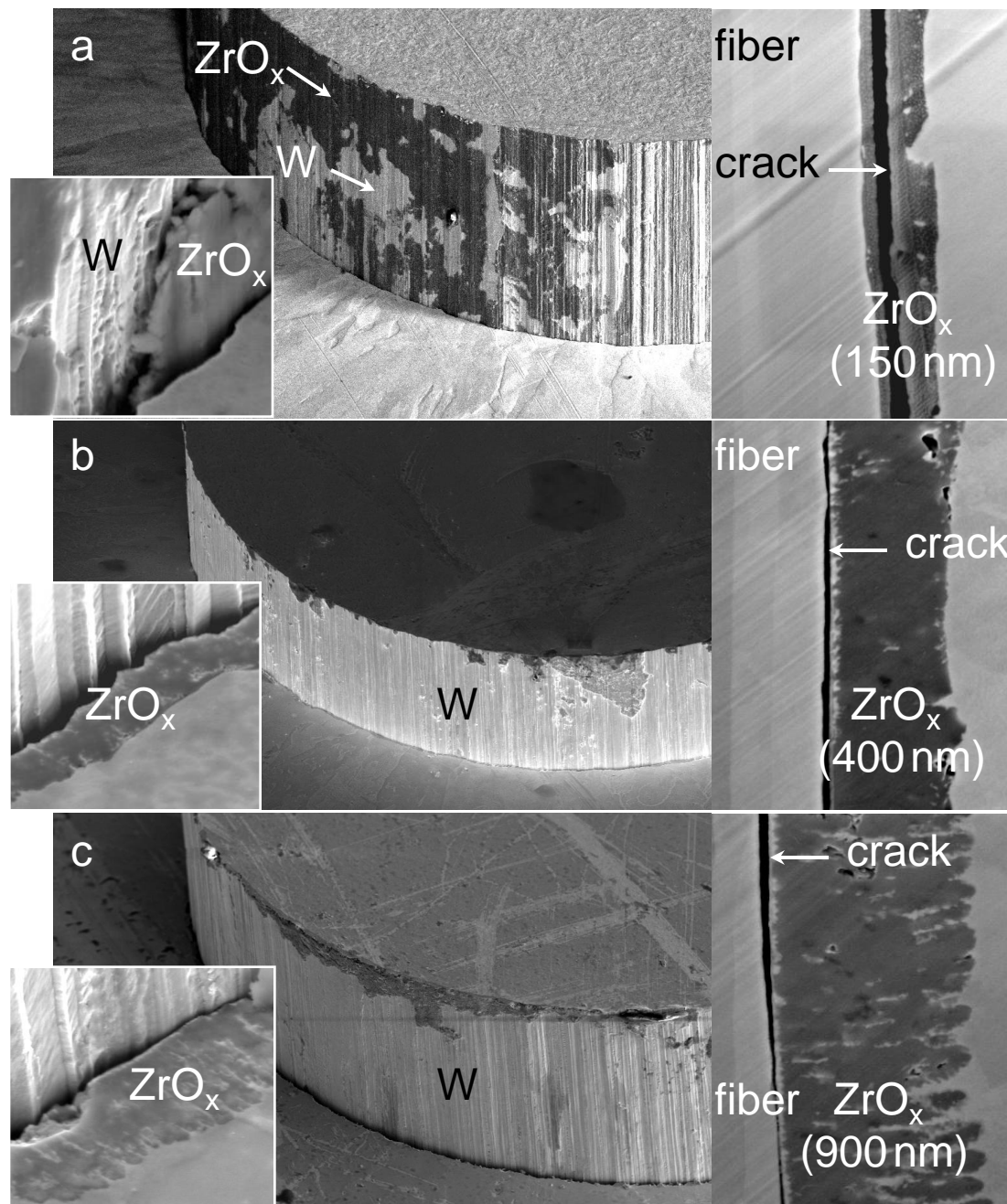


Figure9

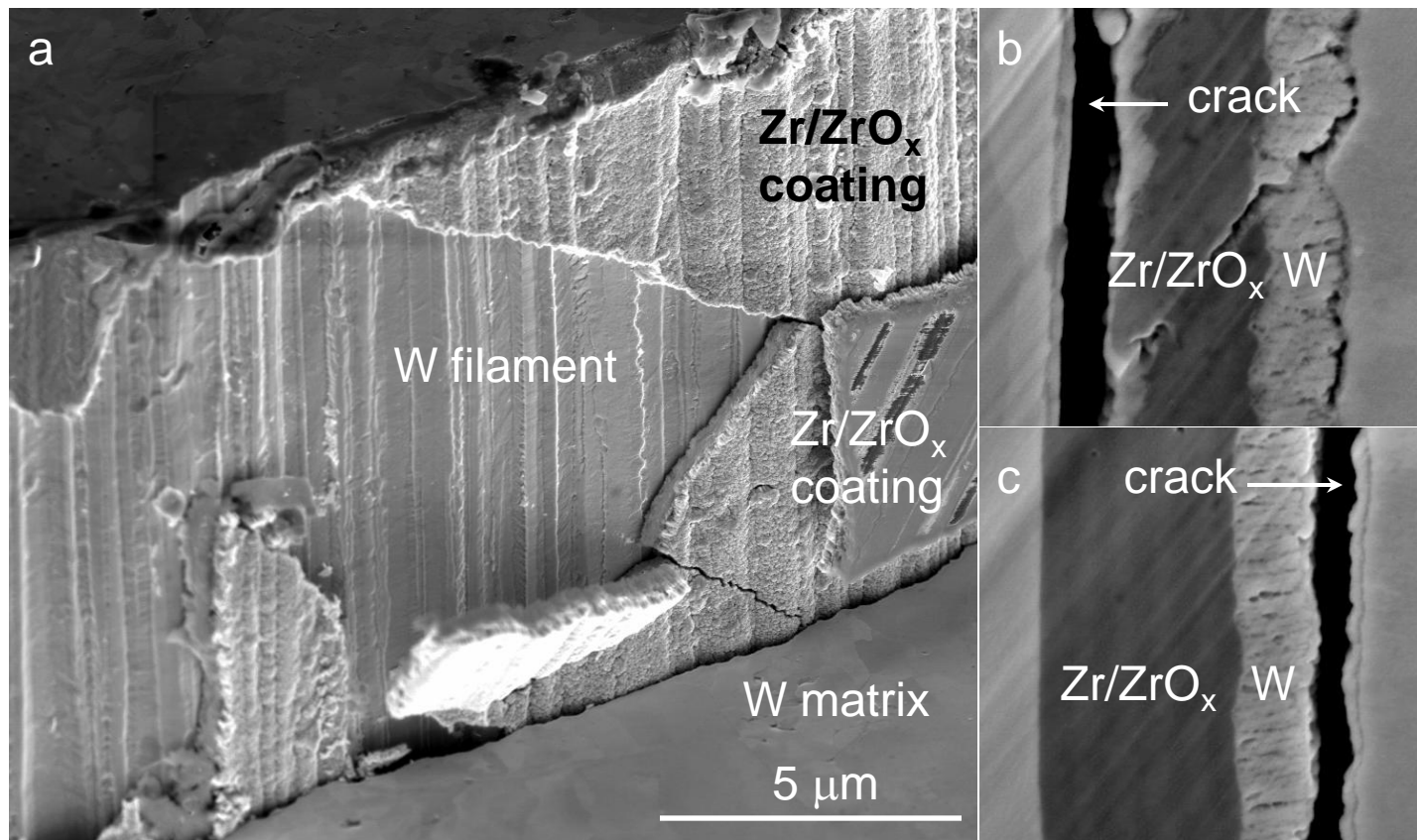


Figure10

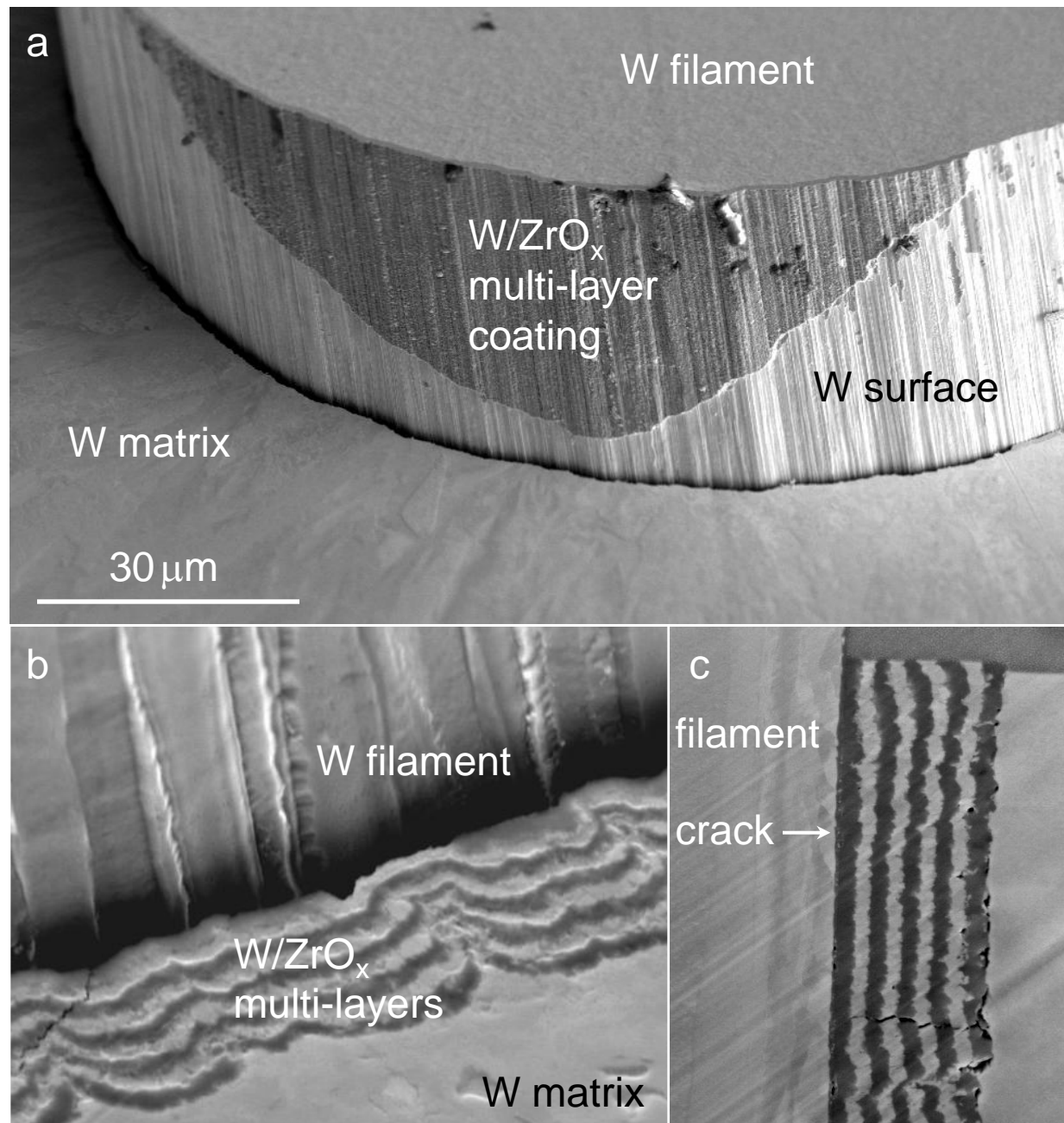


Figure11

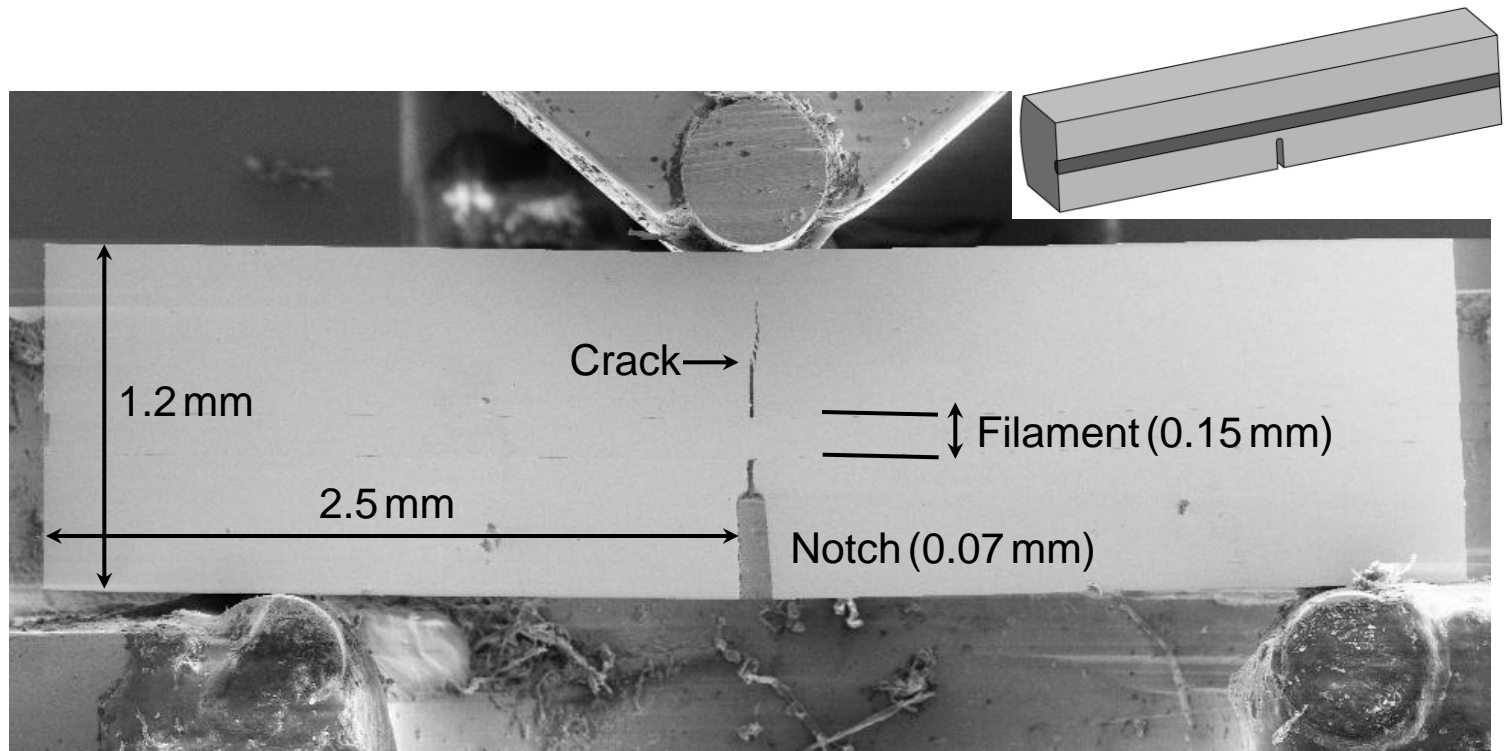


Figure12

